CFD CODE VALIDATION OF ROTOR/FUSELAGE INTERACTION USING THE COMMERCIAL SOFTWARE STAR-CCM+8.04

Boris KUBRAK[1*] and Deryl SNYDER[2]

[1]CD-adapco, 200 Sheperds Bush Road, London W6 7NL, UK

[2]CD-adapco, 2101 Park Center Drive, Suite 290, Orlando, FL 32835, USA

*

past and it has been investigated in numerous experiments [2-6]. Mineck, Raymond and Gorton (NASA) [1] conducted steady and periodic pressure measurements on the fuselage of a generic helicopter model in a wind tunnel. Their now well known ROBIN model experiments are the basis for this CFD code validation study.

Whilst obtaining measurements on the fuselage are relatively easy, it is almost impossible to reveal detailed aerodynamics within or near the rotor disk in experiments. Here numerical analysis (CFD) has a big advantage as the flow can be analysed and visualised anywhere in the domain. The ROBIN case has also been used for validation of non-commercial CFD codes [7, 8, 13].

In this study results predicted by the commercial CFD-software STAR-CCM+8.04 have been validated against the ROBIN experiments [1]. The periodic pressure fluctuations along the centre over the nose and tail boom of the helicopter model were compared to CFD results. Furthermore the vorticity field and isosurfaces of the q-criterion were obtained. The flow structure and the propagation of the blade tip vortices was compared to results obtained from non-commercial CFD codes [7,8].

The air flow has been modelled as a compressible ideal gas. STAR-CCM+ uses a classical Reynolds-Averaged Navier-Stokes Solver (RANS). The conservation equations for mass and momentum have been solved simultaneously with the Coupled Flow Model available in STAR-CCM+8.04 using implicit spatial integration in an unsteady analysis with a coupled algebraic multi-grid method with a courant number of CFL = 30. Turbulence was modelled with the SST-(Menter) k-omega model.

2. CFD SETUP

2.1 Motion Modelling and Mesh

Two methods have been used to model the motion of the rotor:

(a) Sliding interface and morphing mesh
(b) Overset grid

Both methods are capable of modelling superposed motions. In this analysis the main rotor rotation and the cyclic blade pitching has been considered, as these are known parameters that have been measured in the experiments (blade flapping and lead-lag can be neglected as the rotational speed is relatively high at 2000 rpm and centrifugal forces are expected to be dominant in the experiment).

Figure 1 illustrates the two motion modelling approaches employed in this study. The overset mesh method uses 5 grid regions. The grey area is the stationary background mesh that encloses the entire volume in the external air around the fuselage. Because the meshes are unstructured, the background mesh includes the fuselage body as well as the farfield. Each rotor blade is surrounded by its own overset mesh region in the shape of a 'slice' (see Fig. 1 (C)). The overset regions sweep through the stationary background mesh and interpolations are performed at the relevant intersections.

In an overset mesh, cells are grouped into active, inactive, or acceptor cells. Cell designations are updated each time a grid is moved via an automatic

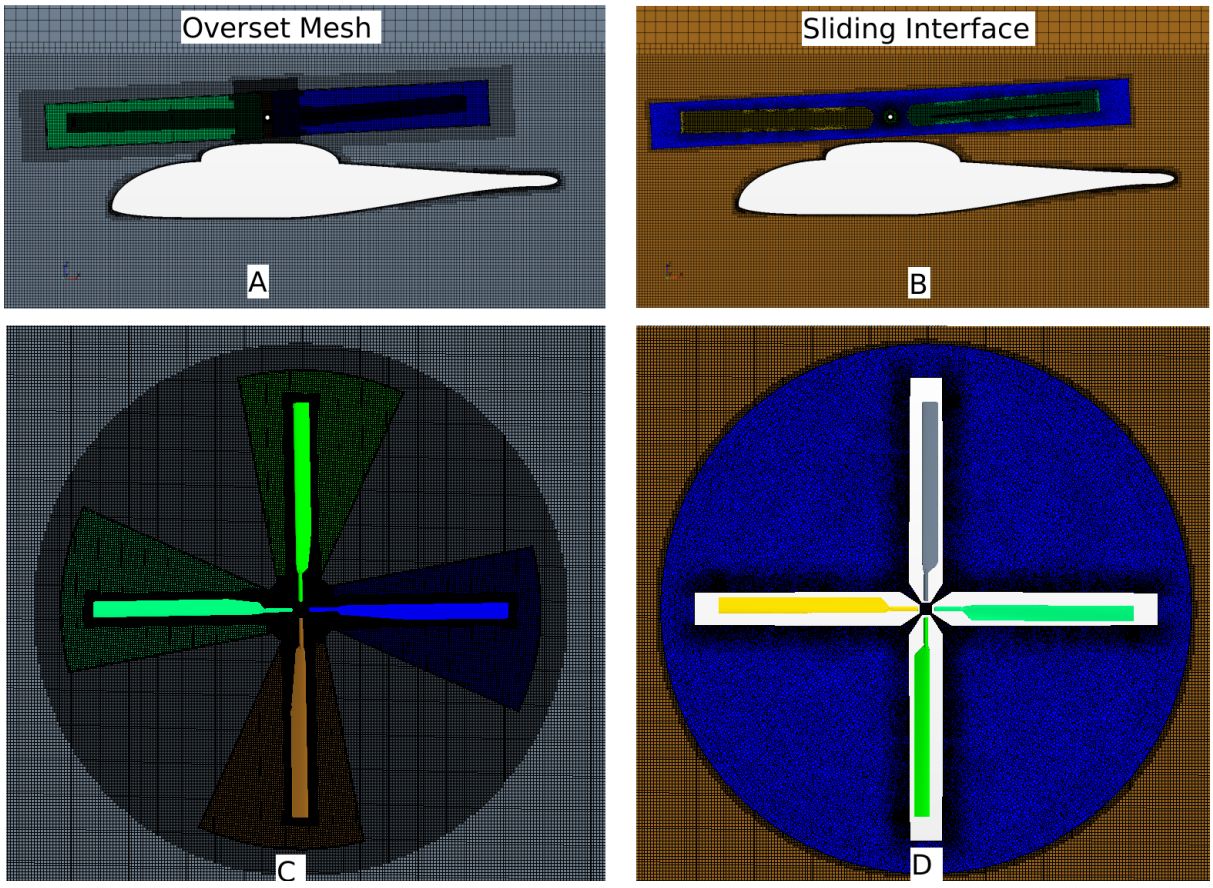

Figure 1: Motion Modelling

hole-cutting algorithm. Within active cells, the discretised governing equations are solved. Within inactive cells, no equation is solved; however, these cells can become active at a later time depending on the motion of the overset regions Acceptor cells separate active and inactive cells, and are attached to the overset boundary in the overset region. Acceptor cells are used to couple solutions on the two overlapping grids. Appropriate entries in the discretised linear system of questions at acceptor cells are provided via interpolation from the neighbouring donor cells. As these interpolations (i.e. shape functions) are included in the linear system, the coupling between grids is fully implicit. Each 'slice' region rotates and exhibits the superposed cyclic pitching motion.

With the Sliding Interface method there are 6 mesh regions. The brown region in Fig. 1 (D) is a stationary mesh encompassing the external air. The blue region models the rotor disk and is a rotating cylindrical mesh region with a sliding interface to the external air. Within this cylindrical mesh region, the mesh is morphed to model the cyclic blade pitching. Each blade lies within a cylindrical region itself that has a rigid mesh. Those cylinders exhibit the cyclic pitching motion and the mesh within the blue main rotor region is morphed. For the purpose of better visualisation the mesh in the cylinders surrounding the blades is not shown in Figure 1 (D).

With both methods the rotation was resolved with 1 degree per time step. The mesh consists of approximately 26 million cells for the Sliding Interface method. The Overset Method uses 45 Million cells. The higher cell count for the overset mesh is due to the preferred practice of keeping similar cell sizes at the interfaces between overset regions. Because the mesh around each rotor blade is refined, the background mesh is refined in the volume where these blades sweep – as visualized in Figure 1 (C). However, it should be noted that active cells are fewer as the grey background cells in figure 1 (A) and (C) become inactive once they lay within the overset 'slice' volume.

The cyclic blade pitch angle Θ is given as a function of the azimuth Ψ as

(1) $$\theta(\psi) = \theta_0 - A_1 cos(\psi) - B_1 sin(\psi)$$

where A_1 = -2.7 deg, B_1 = 2.4 deg and Θ_0 = 10.3 deg.

2.2 Flow Solver

A density-based coupled flow solver has been used for the simulations and a brief description is given here. The coupled solver uses a preconditioned form of the Navier-Stokes equations which in Cartesian integral form for an arbitrary control volume V with differential surface area d_a may be written:

(2) $$\Gamma \frac{\partial}{\partial t}\int_V \mathbf{Q}dV + \oint(\mathbf{F}-\mathbf{G})\cdot d\mathbf{a} = \int_V \mathbf{H}dV$$

Where Q are primitive variables in the Navier-Stokes equations, F are the inviscid terms, G are the viscous terms, H are the body forces and Γ is a preconditioning matrix. Applying equation (2) to a cell-centred control volume for cell-0, one obtains the following discretized system:

(3) $$V_0\Gamma_0\frac{\partial \mathbf{Q}_0}{\partial t} + \sum_f (\mathbf{f}_f + \mathbf{g}_f)\cdot\mathbf{a} = \mathbf{h}V_0$$

Where the summation is over the total number of faces defining cell-0, and f_g and g_f are the inviscid and viscous fluxes through face-f. V_0 is the volume of cell-0 and Γ_0 is the preconditioning matrix that is evaluated in cell-0. A dual-time stepping method, with inner iterations in pseudo-time, is used to recover a time-accurate solution of the preconditioned equations (3) for unsteady flows with implicit time stepping. The preconditioning matrix is a member of Turkel's family of preconditioners. For further reading on the preconditioning and dual-time stepping please refer to the STAR-CCM+ user guide or references [9-11].

2.3 Boundary Conditions and Physical Models

A summary of the boundary conditions is given below:

- Air: ideal gas
- Turbulence Model: SST k-omega, all y+
- Rotor speed: 2000 RPM
- Advance ratio μ = 0.151
- Time step: 1 deg azimuth per time step
- Velocity inlet = $\mu * V_t$ = 27.2 m/s
- Outlet: relative pressure 0 bar
- Ceiling and Floor: Wall
- Sidewalls: Symmetry

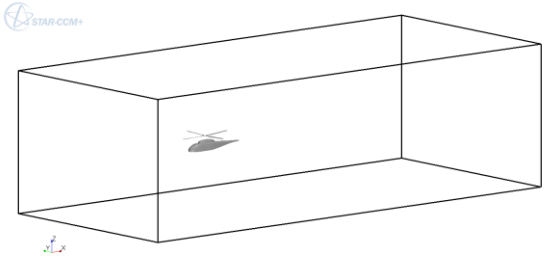

Figure 2: 3D domain

Figure 2 depicts the 3D domain. The size of the domain is the same as the test section used in the wind tunnel [12]. The Sidewalls in the wind tunnel tests were raised out of the flow. It can be assumed there was no effect from the sidewalls and they have been treated in the CFD simulations with the symmetry boundary condition.

3. THE ROBIN HELICOPTER MODEL

The helicopter model was adopted from NASA's well-known wind tunnel experiments on Rotor-Body Interaction (ROBIN). The model consists of a four-bladed driven rotor mounted from the ceiling and a body independently mounted on a post from the floor [1]. In the CFD simulation the mounts have not been modelled and the rotor is modelled as 'floating' without the drive shaft (see figure 2). The blades include link rods that meet near the root as shown in figure 1 (D) to mimic the rotor geometry. The blades have a NACA0012 profile with 8% linear twist. The helicopter model does not include a tail rotor. The fuselage is a generic fuselage model that can be described analytically by super-ellipse equations [1].

3.1 Periodic Pressure Coefficient

The important non-dimensional parameters to describe the rotor aerodynamics are advance ratio μ and thrust coefficient C_T. In the experiments readings from the unsteady pressure transducers were recorded. Mineck and Gordon [1] propose the pressure coefficient to be modified with the advance ratio μ, such that,

(4) $$C_{pmod} = \mu^2 C_p / 2$$

to reflect the effects of the thrust created by the rotor. If the advance ratio is low the flow around the fuselage is dominated by the rotor, not the free stream.
They also found that the magnitude of pressure coefficient fluctuations caused by the rotor increases with the average thrust coefficient C_T. To make the results from the simulations better comparable to the experiments the pressure coefficient should also be corrected by the thrust coefficient. Hence the thrust corrected pressure coefficient reads,

(5) $$C_{pc} = C_{pmod} * C_T / C_{TN}$$

Where C_{TN} = 0.0064 is the average thrust coefficient measured in the wind tunnel and C_T is the average thrust coefficient from the CFD simulations.
The pressure readings used for this validation were taken from 8 locations along the longitudinal centre line as shown in figure 3.

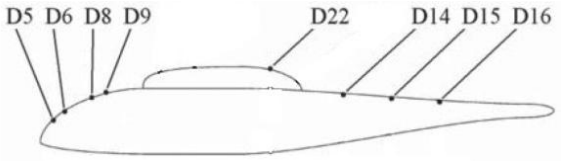

Figure 3: pressure reading locations

4. RESULTS

The CFD simulations were run for five full rotor rotations. After approximately two rotations, the flow becomes quasi-steady, however the simulations were run further until the 5th rotation had completed so that initial disturbances had travelled far enough downstream and the flow was settled. Results shown here are during or after the 5th rotor rotation.

4.1 Vortex Propagation

Figure 4 shows the vorticity field in the central plane section. The range is from 100 to 300 1/s. It can be seen there are two apparent vortex trails in the wake. These are the tip vortices once shed when the blade tip passes through the plane section over the nose and once when the blade tip passes through the plane section over the tail boom. When the tip vortices are released over the tail boom the vortices are located almost directly above the vortex trail that originates over the nose. The vortices are rotating in opposite sense; hence they enhance each other and maintain momentum, enabling a long propagation far downstream.

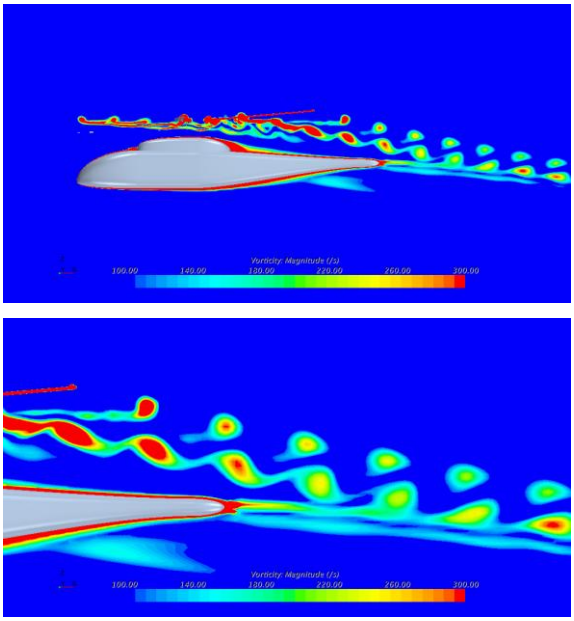

Figure 4: Overset Case: Vorticity Field in central plane

4.1 Code-to-Code Comparison of Isosurface Plots

To trace the propagation of vortices the Q-criterion is a good measure. It allows a qualitative judgement of the flow features around the helicopter and is a good method to locate vortices. Isosurfaces for the Q-criterion of 0.05 have been created after 5 rotor rotations. The results are shown in figure 5 (a). Figure 5 (b) shows a comparison of isosurfaces obtained from the rFlow3D code developed by the Japan Aerospace Exploration Agency (JAXA) [7]. The isosurfaces obtained with STAR-CCM+ are in very good agreement with isosurfaces predicted by rFlow3D. Both codes predict very similar vortex

propagation. The modified pressure coefficient C_{Pmod} is plotted on the isosurfaces in figure 5 (a) ranging from -1.5 to 1.

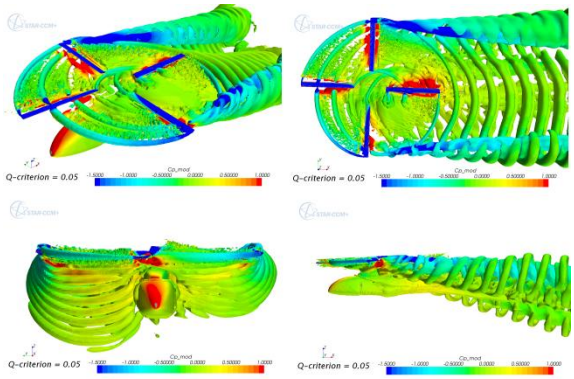

(a) STAR-CCM+8.04

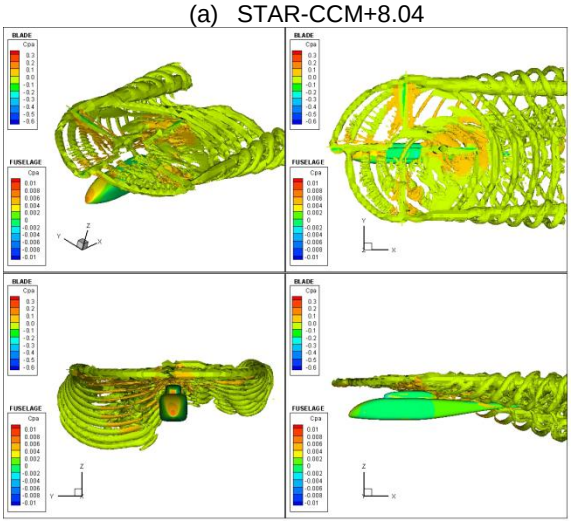

(b) rFlow3D [7]

Figure 5: Code-to-Code comparison of q-criterion isosurfaces from overset case (Q-criterion = 0.05)

4.1 Thrust Coefficient

Figure 6 shows a plot of the thrust coefficient C_T during the first 5 rotor rotations. After around two rotations the thrust becomes periodic with a peak in thrust every 90 degrees due to the blade passage. In the experiments the thrust fluctuations was not measured and only the average thrust was measured.

The two motion modelling techniques delivered two different thrust coefficients which where slightly below and above the experimental value. When averaging the thrust coefficient for the 5th rotor rotation the Sliding Interface method delivered an average of C_T = 0.00607, the Overset method delivered C_T = 0.00702 whereas the experimental value was between at C_{TN} = 0.0064. This allows the calculation of the thrust corrected pressure coefficient in equation (5).

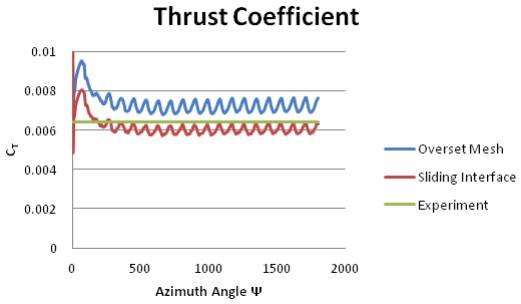

Figure 6: Thrust Coefficient

4.2 Unsteady Pressure Coefficient on Fuselage

The pressure coefficient was monitored along the longitudinal centre line over the nose and tail boom. The average thrust coefficients from figure 6 have been used to calculate the pressure coefficient given in equation (5). Figure 7 shows the results for a full rotor rotation at four locations over the nose. The plots clearly depict the pressure pulses due to the passage of the four rotor blades. At the foremost location D5 the pressure coefficient predicted by the CFD simulations is higher however the magnitude of the amplitude is very similar to the experiments.

Figure 8 shows the unsteady pressure coefficient at four locations over the tail boom. It is evident that the flow field is more disturbed because these locations are in the wake of the rotor and passed by the tip vortices. In Figure 4 the vortex propagation is visualized and it can be seen that the tail boom is in proximity of the blade tip vortices. The flow field is also disturbed by the cowling on the top of the fuselage. This is also reflected in the pressure coefficient readings at these locations (Figure 8) which are more irregular than over the nose (Figure7).

Generally the CFD results are in good agreement and the magnitude of the pressure variations is very similar to the experiments, however the total level in some areas is higher. Both motion modelling techniques provide very similar results. The CFD results are predicting a higher pressure coefficient nearer to the nose and at the far end of the tail boom. This is a trend that was also found in other CFD validation studies using the ROBIN wind tunnel experiments [7, 8, 13].

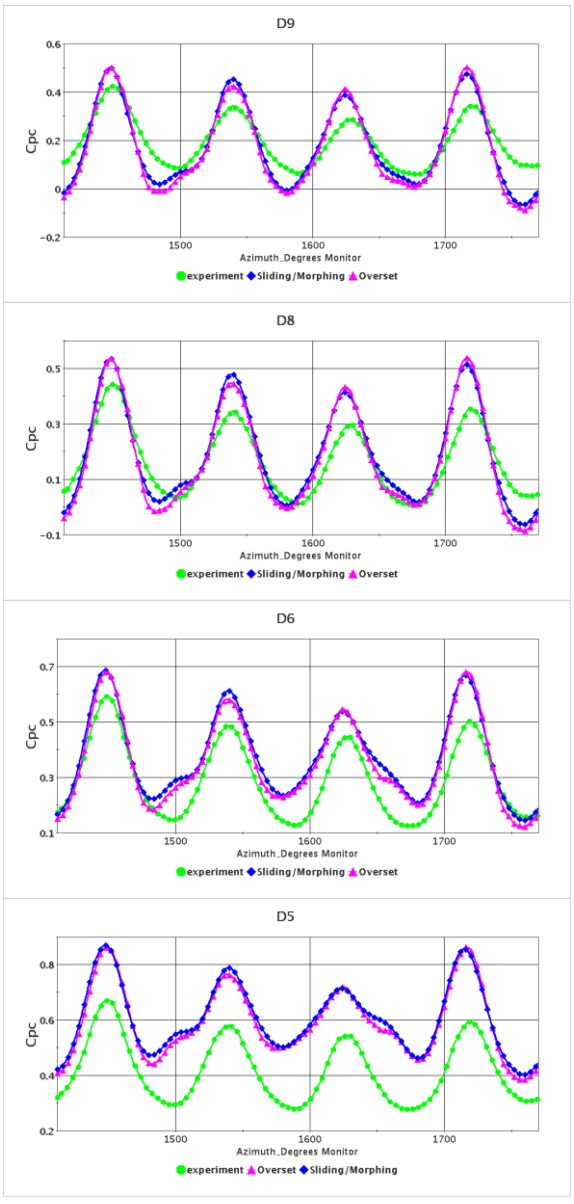

Figure 7: Pressure Coefficient over the nose

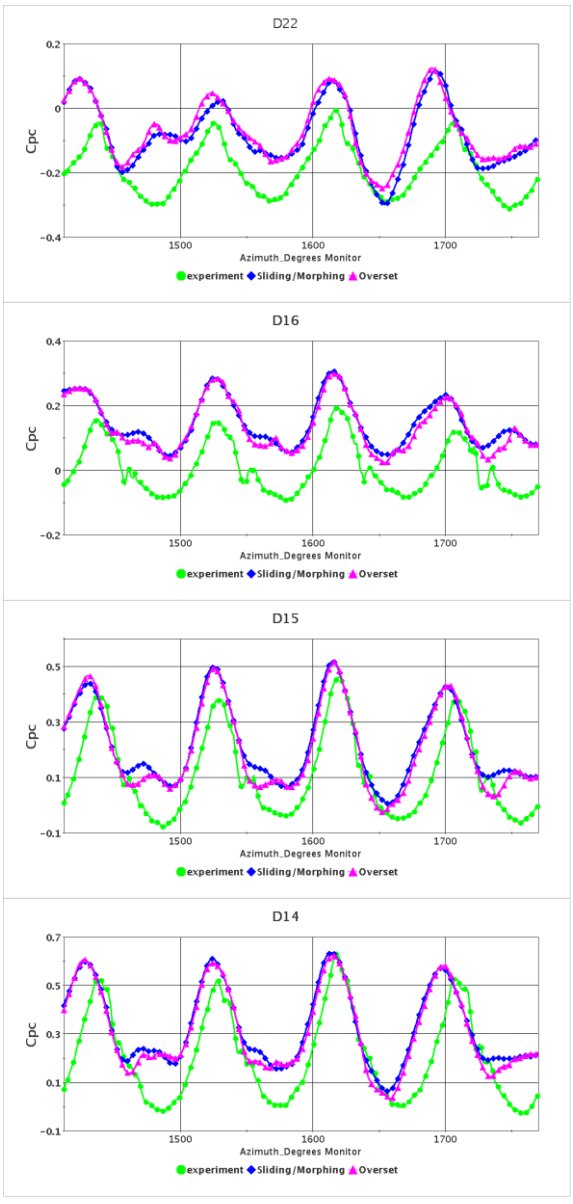

Figure 8: Pressure coefficient over the tail boom

5. CONCLUSIONS

A computational analysis of helicopter interactional aerodynamics has been carried out using the commercial software STAR-CCM+ 8.04. Two motion modelling methods have been compared, one using a Sliding Interface approach and the other using the Overset Mesh method. Both methods deliver nearly identical results.

The CFD simulations revealed detailed propagation of the tip vortices downstream which are qualitatively in good agreement with a non-commercial CFD-code [7].

The unsteady pressure coefficients were monitored at locations along the centreline of the fuselage and the results were compared to wind tunnel experiments to validate the CFD results. There is generally a good agreement with the experiments. The magnitude of the variations due to the blade passage is very similar between numerical results and wind tunnel experiments, however the pressure is generally overpredicted at the front of the nose and at the far end of the tail boom. This is a trend in accordance with validation studies of other CFD-codes [7, 8, 13].

The motion modelling techniques provided with STAR-CCM+ deliver very similar results and a deeper insight into the complex aerodynamics of helicopters can be gained. The overset method is very flexible and much more complex motion including blade flapping and lead-lag could be prescribed. Especially within or near the rotor where experimental measurements are difficult the CFD method can be a powerful tool to gain an understanding into the complex flow field.

6. REFERENCES

[1] Mineck, Raymond E., and Susan A. Gorton. *Steady and periodic pressure measurements on a generic helicopter fuselage model in the presence of a rotor*. No. NASA-L-17962. NATIONAL AERONAUTICS AND SPACE ADMINISTRATION HAMPTON VA LANGLEY RESEARCH CENTER, 2000.

[2] McMahon, H. M.; Komerath, N. M.; and Hubbartt, J. E.: *Studies of Rotor-Airframe Interactions in Forward Flight.* AIAA paper 85-5015, October, 1985.

[3] Leishman, J. G.; and Bi, Nai-pei: Aerodynamic Interactions Between a Rotor and a Fuselage in Forward Flight. *Proceedings of the 45th Annual Forum of the American Helicopter Society.* May, 1989.

[4] Crouse, G. L., Jr.; Leishman, J. G.; and, Bi, N.: Theoretical and Experimental Study of Unsteady Rotor/Body Aerodynamic Interactions. *Journal* of *the American Helicopter Society,* Vol. 37, No. 1, Jan. 1992, pp. 55-65.

[5] Modersheim, E.; and, Leishman, J. G.: Investigation of Aerodynamic Interactions Between a Rotor and a T-Tail Empennage. *Journal* of *the American Helicopter Society,* Vol. 43, No. 1, January, 1998, pp. 37-46.

[6] Berry, John; and Bettschart, Nicolas: Rotor-Fuselage Interaction: Analysis and Validation with Experiment. *Proceedings of the 53rd Annual Forum of the American Helicopter Society.* May, 1997

[7] TANABE, Yasutada, Shigeru SAITO, and Ippei OTANI. "Validation of Computational Results of Rotor/Fuselage Interaction Analysis Using rFlow3D Code." JAXA Research and Development Report 10 (2010): 1-14.

[8] Steijl, R., and G. N. Barakos. "Computational Study of Helicopter Rotor-Fuselage Aerodynamic Interactions." *AIAA journal* 47.9 (2009): 2143-2157.

[9] Turkel, E. 1987. “Preconditioned methods for solving the incompressible and low speed compressible equations”, Journal of Computational Physics, 72, pp. 277-298.

[10] Weiss, J.M., Maruszewski, J.P., and Smith, W.A. 1999. “Implicit solution of preconditioned Navier-Stokes equations using algebraic multigrid”, AIAA Journal, 37(1), pp. 29-36.

[11] Weiss, J.M., and Smith, W.A. 1995. “Preconditioning applied to variable and constant density flows”, AIAA Journal, 33(11), pp. 2050-2057.

[12] Gentry, Garl L. Jr.; Quinto, E Frank; Gatlin, Gregory M.; and Applin, Zachary T.: *The Langley 14- by 22-Foot Subsonic Tunnel: Description, Flow Characteristics, and Guide for Users.* NASA TP 3008. September 1990.

[13] H.J. Nam, Y. Park, and O.J. Kwon. Simulation of unsteady rotor-fuselage aerodynamic interaction using unstructured adaptive meshes. J. American Helicopter Society, 51(2):141–148, 2006